Condensation, excitation, pairing, and superfluid density in high-T_c superconductors: the magnetic resonance mode as a roton analogue and a possible spin-mediated pairing

2004 J. Phys.: Condens. Matter 16 S4515

(http://iopscience.iop.org/0953-8984/16/40/007)

INSTITUTE OF PHYSICS PUBLISHING JOURNAL OF PHYSICS: CONDENSED MATTER

J. Phys.: Condens. Matter **16** (2004) S4515–S4540 PII: S0953-8984(04)85101-4

Condensation, excitation, pairing, and superfluid density in high-T_c superconductors: the magnetic resonance mode as a roton analogue and a possible spin-mediated pairing

Y J Uemura

Physics Department, Columbia University, 538 West 120th Street, New York, NY 10027, USA

Received 23 April 2004
Published 24 September 2004
Online at stacks.iop.org/JPhysCM/16/S4515
doi:10.1088/0953-8984/16/40/007

Abstract

To find a primary factor determining T_c and a pairing mechanism in high-T_c cuprates, we combine the muon spin relaxation results on n_s/m^* (superconducting carrier density/effective mass), accumulated over the last 17 years, with the results from neutron and Raman scattering, scanning tunnelling microscopy, specific heat, Nernst effect, and angle-resolved photoemission spectroscopy measurements. We identify the neutron magnetic resonance mode as an analogue of the roton minimum in the superfluid ^{4}He, and argue that n_s/m^* and the resonance mode energy $\hbar\omega_{res}$ play a primary role in determining T_c in the underdoped region. We propose a picture wherein roton-like excitations in the cuprates appear as a coupled mode, which has resonance modes for spin and charge responses at different momentum transfers but the same energy transfer, as detected respectively by means of the neutron $S = 1$ mode and the Raman $S = 0\,A1_g$ mode. We shall call this the 'hybrid spin/charge roton'. After discussing the role of dimensionality in condensation, we propose a generic phase diagram for the cuprates with spatial phase separation in the overdoped region as a special case of the Bose–Einstein to Bardeen–Cooper–Schrieffer crossover conjecture where the superconducting coupling is lost rapidly in the overdoped region. Using a microscopic model of charge motion resonating with antiferromagnetic spin fluctuations, we propose the possibility that the hybrid spin/charge roton and higher-energy spin fluctuations mediate the superconducting pairing. In this model, the resonance modes can be viewed as a meson analogue and the 'dome' shape of the phase diagram can be understood as a natural consequence of departure from the competing Mott insulator ground state via carrier doping.

1. Introduction

Since the discovery of high-T_c superconductors (HTSC), muon spin relaxation (μSR) measurements[1] [2, 3] have been used to study magnetic order, superconducting penetration depth, and flux vortex aspects of the cuprates and other exotic superconductors. We have particularly focused on the absolute values of the magnetic field penetration depth λ, which represents the superconducting carrier density n_s divided by the effective mass m^* as $\lambda^{-2} \propto n_s/m^*$. We discovered strong and universal correlations between the critical temperature T_c and $n_s/m^*(T \to 0)$ in various HTSC systems [4], and initiated an energy-scale argument by converting n_s/m^* into an effective Fermi temperature T_F of the superconducting carriers [5]. Combining the universal correlations and the pseudogap behaviour, we proposed a picture for the cuprates based on crossover from Bose–Einstein (BE) to Bardeen–Cooper–Schrieffer (BCS) condensation, in 1994 [6, 7]. We also demonstrated that the correlations between T_c and n_s/m^* are robust against various artificial/spontaneous formations of spatial heterogeneity, such as Cu/Zn substitution, for which we proposed the 'Swiss cheese model' in 1996 [8].

During recent years, after 1997, several important experimental results on the cuprates, relevant to the above-mentioned results/pictures, have been obtained by using other techniques. They include:

(1) scanning tunnelling microscope results which confirmed the 'swiss-cheese'-like situation in Zn doped cuprates [9], and further established spontaneous formation of spatial heterogeneity in the superconducting state over a wide range of doping levels even without impurity substitution [10, 11];
(2) high-frequency conductivity measurements of n_s/m^*, which showed a frequency-dependent 'dynamic' response remaining above T_c and provided the first direct evidence for a wide range of superconducting phase fluctuations in the normal state [12];
(3) the Nernst effect measurements which provided further evidence for the dynamic superconducting response above T_c, and mapped out the region of this response as a function of external field H, temperature T, and the doping concentration x [13, 14];
(4) neutron scattering studies which established that the '41 meV magnetic resonance mode', first found in YBCO [15], is generic to many of the cuprate systems, and that the mode energy accurately scales with T_c [16–18];
(5) Raman scattering studies which obtained the response in the $A1_g$ mode at $T \to 0$ whose energy precisely follows that of the neutron resonance peak [19–22]; and
(6) a sharp 'coherence peak' which appears in the antinodal response of ARPES studies, with the intensity proportional to the superfluid density [23].

In this paper, we wish to demonstrate that the combination of the μSR results with the new results (1)–(6) can clarify the primary determining factor for the critical temperature T_c in the cuprates and can elucidate details of their superconducting condensation and pairing mechanisms. This discussion will proceed with a comparison with known cases of quantum superfluid transitions in bulk and thin films of liquid ^{4}He. In particular, we will propose a picture wherein the 41 meV resonance mode in the cuprates plays a role analogous to that of rotons in liquid He, as the key elementary excitation mode which determines T_c. We further propose a picture of a 'hybrid spin/charge roton' in an effort to reconcile apparently conflicting selection rules for the neutron magnetic resonance mode and the Raman $A1_g$ mode, which are observed with the same energy transfer [19].

[1] For general aspects and the historical development of the μSR approach, see the proceedings of nine international conferences on muon spin rotation/relaxation/resonance [1].

Consideration of dimensionality effects will lead to a new and simple account for the onset temperature of the Nernst effect and conditions necessary for dynamic superconductivity. We will compare evidence for phase separation in the overdoped cuprates, and argue that the condensation in the cuprates can be viewed as a special case of BE–BCS crossover where the pairing interaction vanishes in a moderately overdoped region. Finally, we consider a microscopic model where the motion of a charge is assisted by spin fluctuations having the *same resonating frequency*. Developing this notion, we propose a picture wherein the 'hybrid spin/charge roton' and higher-energy antiferromagnetic (AF) spin fluctuations can be the pair mediating bosons. These concepts naturally lead to a view in which we ascribe the anomalies in the overdoped region to the rapid disappearance of spin fluctuations due to increasing distance from the Mott AF insulator state.

2. Plots of T_c versus n_s/m^* and T_c versus T_F

In the vortex state of type-II superconductors, the applied field H enters into the system by forming a lattice of flux vortices, with a typical distance between the adjacent vortices $\sim$1000 Å for $H \sim 1$ kG. The vortex lattice and supercurrent create inhomogeneity ΔH in the internal magnetic fields, whose decay from the vortex core position is related to the London penetration depth λ. For μSR measurements, a time histogram is composed of the precession of 10^6–10^7 muons stopped at locations of different internal fields. In measurements with ceramic specimens, the damping of the precession envelope is often approximated by a Gaussian function $\exp(-\sigma^2 t^2/2)$, which defines the muon spin relaxation rate $\sigma \propto \Delta H$. With the London equation, one finds

$$\sigma \propto \lambda^{-2} = [4\pi n_s e^2/m^* c^2][1/(1+\xi/l)], \tag{1}$$

where ξ is the coherence length and l denotes the mean free path. In systems in the 'clean limit' with $\xi \ll l$, such as the cuprates, σ represents n_s/m^*.

Figure 1 shows our accumulated results obtained over the last 15 years in a plot of T_c versus $\sigma(T \to 0) \propto n_s/m^*$ for various cuprate systems [4, 5, 8, 24–27]. These data are consistent with results from other groups [28–31]. We see that T_c increases with increasing carrier doping, following a nearly linear relationship with n_s/m^* in the underdoped region: the results from different series of cuprates share a common slope for this initial increase of T_c. Systems in the optimally doped region deviate from this linearity, showing a 'plateau'-like behaviour, which was later found out to be due to the effect of the CuO chains in the case of the YBCO systems [29]. We see that the nearly linear trend is followed also by systems with Cu/Zn substitution [8], spontaneous formation of static magnetic regions (shown with the 'stripe' symbols), and even with overdoping (Tl2201) [24], the implications of which will be discussed in later sections.

Strong correlations between T_c and n_s/m^* would not be expected from BCS theory [32], but are readily expected in BE condensation. Thus, this figure gives the first strong message about possible non-BCS character of condensation in the cuprates. In fact, when one assumes m^* for the cuprates to be 3–4 times the bare electron mass, the carrier density n_s for systems in the linear region corresponds to the situation where several pairs are overlapping within an area of $\pi\xi^2$ on the CuO_2 planes, which interpolates between non-overlapping pairs in the BE limit and thousands of pairs per $\pi\xi^2$ in the BCS limit [33]. Although most of the points in figure 1 were obtained with unoriented ceramic specimens, the results predominantly reflect the in-plane penetration depth and the in-plane mass, as generally demonstrated for highly anisotropic superconductors [34], with a $\sim$40% correction factor between the relaxation rates from unoriented and oriented (or single-crystal) specimens.

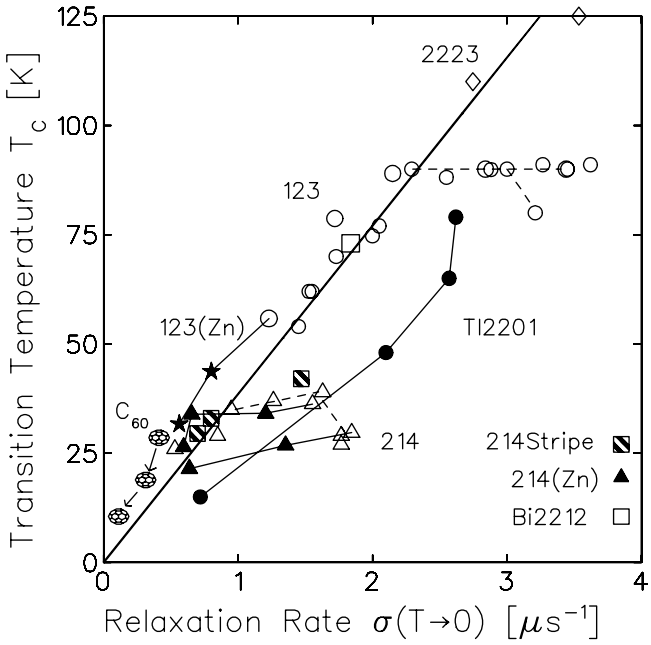

Figure 1. The muon spin relaxation rate $\sigma \propto n_s/m^*$ at $T \to 0$ for various high-T_c cuprate superconductors [4, 5, 8, 24–27] and A_3C_{60} systems [35, 36] plotted against the superconducting transition temperature T_c. The points for HTSC with open symbols represent simple hole doped systems, while closed triangles are for (Cu, Zn) substitution [8], 'stripe' symbols for systems with the formation of island regions with incommensurate static spin modulations [25], and closed circles for overdoped Tl2201.

The parameter n_s/m^* in equation (1) represents the spectral weight of the three-dimensional screening supercurrent which causes a partial rejection of the applied field. Knowing the average interlayer distance c_{int} between the CuO_2 planes, one can obtain the 2D area density n_{s2D} of superconducting carriers, which can be directly converted into the effective Fermi temperature $T_F \propto n_{s2D}/m^* = n_s/m^* \times c_{int}$. For 3D systems, the $\sigma \propto n_s/m^*$ results have to be combined with those on the Pauli susceptibility or Sommerfeld constant $\gamma \propto n^{1/3}m^*$ in the derivation of $T_F \propto n_s^{2/3}/m^*$. After this processing, we produced a plot of T_c versus T_F first in 1991 [5]. Figure 2 shows the up-to-date version of this plot, including subsequent data for various different superconductors [33, 35–39].

The T_B line represents the BE condensation temperature of an ideal Bose gas of boson mass $2m^*$ and density $n_s/2$. Although the actual superconducting T_c of the cuprates are reduced by a factor of 4–5 from T_B, the trend of the underdoped cuprates is parallel to the T_B line, suggesting that the linear trend could be deeply related to BE condensation. There seems to be an empirical upper limit of T_c/T_F shared not only by the cuprates but also by other strongly correlated systems, such as organic 2D bis(ethylene-dithio)tetrathiafulvalene (BEDT) [37], Na_xCoO_2 [39], and A_3C_{60} [35, 36] systems. Figure 2 serves for classifying different superconductors between the limits of BE condensation with strong coupling (approaching towards the T_B line) and BCS condensation with much smaller values of T_c/T_F.

In figure 2, we also include a point for superfluid bulk ^{4}He with $T_c = 2.2$ K (blue star). Even for such a system regarded as a prototype for BE condensation, we see a 30% reduction from its ideal-gas value of $T_{BE} = 3.2$ K, presumably caused by the finite size and interactions of He atoms. In addition to these factors, two-dimensional aspects of the cuprates could also

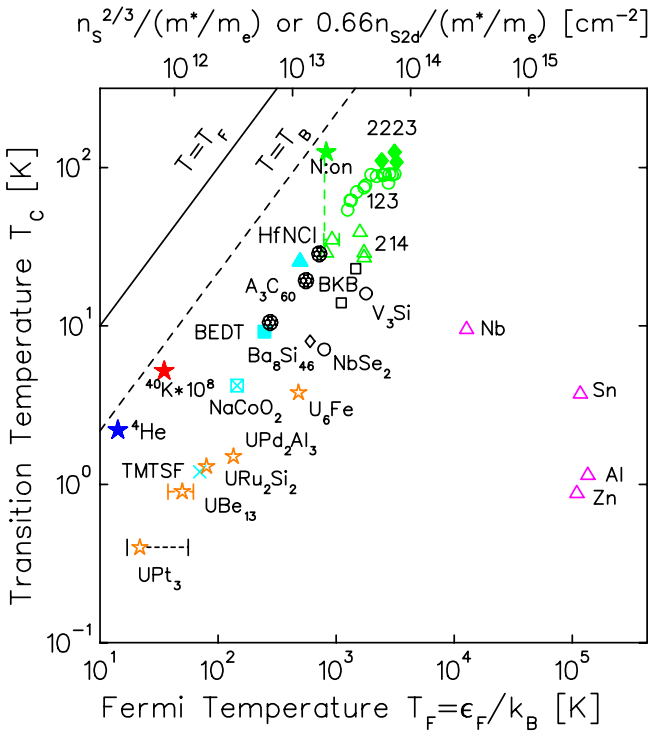

Figure 2. A plot of T_c versus the effective Fermi temperature T_F obtained from the superfluid response n_s/m^* of various superconducting systems, first attempted in [5] in 1991, and updated to include results from [4, 5, 35–39]. We see an empirical upper limit $T_c/T_F \sim 0.05$ for superconducting systems. Also included are the corresponding points for the superfluid ^{4}He (blue star) and the ultracold ^{40}K [40] in the BE–BCS crossover region (red star; with T_c and T_F both multiplied by 10^8). The T_B line shows the BE condensation temperature for the ideal Bose gas of boson density $n_s/2$ and mass $2m^*$. The green star represents the onset temperature T_{on} of the Nernst effect, shown in figure 8(b), for $La_{1.9}Sr_{0.1}CuO_4$ [13, 14], which represents the case for 'hypothetical 3D and roton-less underdoped LSCO'.

cause a further reduction of T_c from T_B as discussed in section 5. Recently, condensation of fermionic ultracold ^{40}K gas has been achieved in the BE–BCS crossover region [40]. We also plot a point for ^{40}K (red star) by multiplying both T_c and T_F by 10^8. Interestingly, the crossover region seems to exist rather close to the T_B line for the case of ultracold fermion atoms, for which we expect a much smaller effect of correlations compared to the cuprates.

3. The BE–BCS crossover conjecture

The connection between BE and BCS condensation has been a subject of theoretical interest for many decades. There exist a few different energy scales for superconductivity: (a) the energy of condensing carriers represented by T_F, related to the number density and mass; (b) the net attractive interaction, related to the gap energy scale on the BCS side, and to the binding energy in local bosons; and (c) the energy of 'pair mediating bosons' such as the Debye frequency in the phonon coupling. For a fourth energy scale (d), the condensation temperature T_c is determined by the interplay among (a)–(c). Many theoretical discussions have been given, fixing the carrier concentration (a), and artificially changing the attractive coupling (b). As

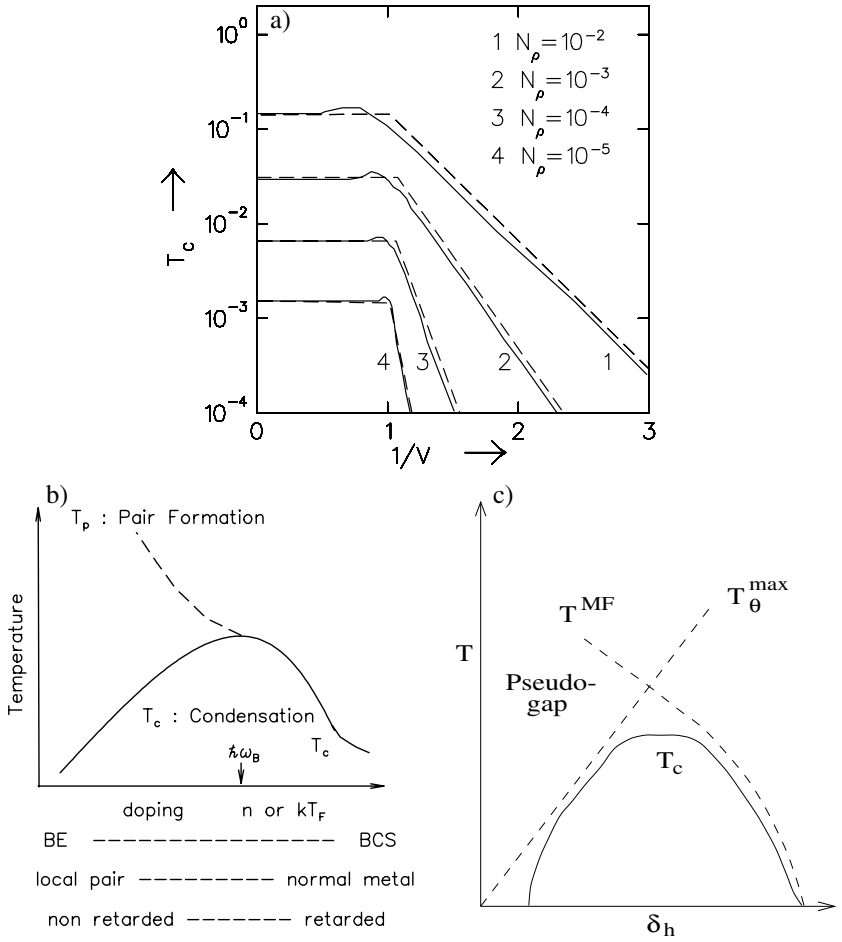

Figure 3. (a) The transition temperature T_c plotted against the inverse of the normalized attractive coupling strength V in the BE–BCS crossover region obtained by Nozières and Schmitt-Rink [41] in 1984 for various particle densities. Since V is defined with parameters including N_p, the N_p dependence for fixed interaction strength cannot be directly obtained from this figure. (b) The BE–BCS crossover picture proposed by Uemura [6, 7] in 1994 with the crossover region characterized by the matching of kinetic energy $k_B T_F$ of the condensing carriers with the mediating boson energy $\hbar\omega_B$. When one identifies the pair formation temperature T_p as the pseudogap temperature T^*, this phase diagram can be mapped to the case of HTSC. (c) A phase diagram based on the superconducting phase fluctuations in the pseudogap region proposed by Emery and Kivelson [45] (reproduced by permission of Nature Publishing Group http://www.nature.com) in 1995 as an explanation to the relationship shown in figure 1. T^{MF} represents the mean-field attractive interaction, while T_θ^{max} shows the maximum temperature up to which the superconductivity in 2D systems can survive against thermal excitations of phase fluctuations.

a typical example, figure 3(a) shows the results obtained by Nozières and Schmitt-Rink [41] in 1985. Note that the horizontal axis is given for the coupling strength V, normalized to the 'critical strength' V_c related to the particle density and the range of the interaction. We see that $T_c \sim T_B$ in the strong coupling limit ($1/V < 1$), while $T_c \propto V$ on the BCS side ($1/V \gg 1$).

In cuprate systems, we change the carrier density (a), while the attractive energy scale (b) is not necessarily fixed. On the other hand, the 'mediating boson' would not change for different carrier densities. So, it would make sense to consider the case of fixing (c) and varying (a),

and consider how (b) and (d) would evolve. By combining the results in figures 1 and 2 with the pseudogap behaviour which was then noticed in NMR (spin gap) [42, 43] and c-axis conductivity [44] (insulating below T^*) studies, we proposed a picture shown in figure 3(b) in 1994 [6, 7] for mapping the situation of the cuprates to BE–BCS crossover. We argued that the underdoped region corresponds to the BE side, where the pair formation temperature $T_{\rm pair}$ maps to T^*, below which one expects gradual formation of spin singlet pairs. On the BCS side $T_{\rm pair}$ and T_c should be very close, since the condensation occurs immediately after the pair formation. These two regions may be separated by whether the interaction is non-retarded (BE side) or retarded (BCS side).

Emery and Kivelson [45] presented the phase fluctuation picture, independent from our picture, shown in figure 3(c) in 1995, and interpreted the μSR results as a signature for a Kosterlitz–Thouless (KT) type of transition [46] expected in two-dimensional systems where superconductivity is destroyed by thermal excitations of phase fluctuations. Although their picture in figure 3(c) shares various fundamental aspects with the BE–BCS crossover pictures, some important differences exist, as discussed in later sections. The overdoped region of the cuprates, which corresponds to the 'BCS' side of figures 3(b) or (c), turns out to be quite different from the simple BCS systems, as discussed in section 8. Various kinds of models based on BE condensation [47, 48] and BE–BCS crossover [49] have also been proposed to account for HTSC.

4. Heterogeneity

The relevance of BE condensation also appears in the robustness of the cuprates against heterogeneous spatial media. The first signature of this was seen in our study of Zn doped YBCO and LSCO systems in 1996 [8]. As shown in figure 4(a), the reduction of n_s/m^*, as a function of Zn concentration, can be explained very well if we assume that Zn creates a non-superconducting region around it in an area of $\pi\xi^2$ on the CuO_2 planes. The solid curve in figure 4(a), representing this 'Swiss cheese model', agrees well with the data *without any fitting*. A few years later, this situation was directly confirmed by scanning tunnelling microscope (STM) studies [9], as shown in figure 4(b).

In Eu doped $(La, Eu, Sr)_2CuO_4$ (LESCO), regions with static incommensurate magnetic order are formed spontaneously even in superconducting specimens [26]. The volume fraction of regions with static magnetic order shows a one-to-one trade-off with the total value of n_s/m^*, as shown in figure 4(c), indicating that the 'magnetic island' regions do not support superfluid. Thus the situation looks again like the 'Swiss cheese', with 'non-superconducting magnetic islands' replacing the 'normal area around Zn'. In zero-field μSR measurements of oxygen overdoped $La_2CuO_{4.11}$ [25], we found the average size of such magnetic islands to be comparable to the in-plane coherence length $\xi \sim 15$–30 Å in radius. The Zn doped and magnetic island systems follow the same trend as other less perturbed underdoped cuprates in figure 1.

Recently, spontaneous formation of spatially heterogeneous areas, with similar length scales, was discovered by a series of STM measurements [10, 11] on underdoped to optimally doped Bi2212 systems without impurity doping. As shown in figure 4(d), the STM 'gap map' clearly demonstrates a decomposition of the system into regions with a sharp superconducting gap (orange to red colours) and a broad pseudogap-like response (blue to black colours). Upon doping with carriers, the former region increases in volume fraction, which roughly follows the behaviour of n_s/m^* [50]. The new STM results suggest the possibility that the underdoped cuprates are analogous to 'spontaneously formed Swiss cheese'. We shall see later that overdoped Tl2201 also exhibits yet another type of spatial heterogeneity/phase separation.

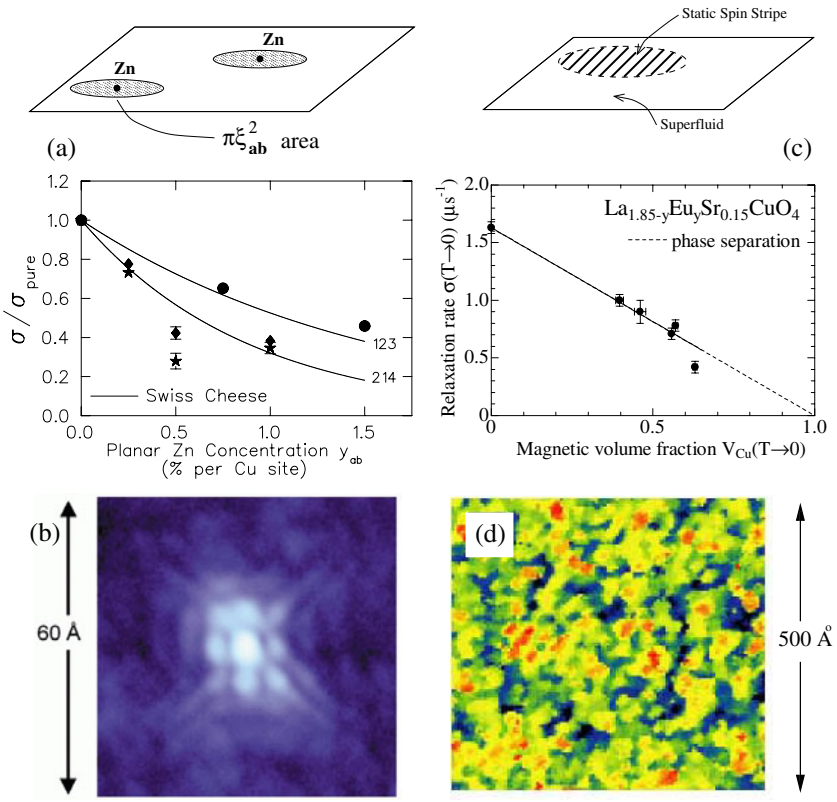

Figure 4. (a) The muon spin relaxation rate $\sigma(T \rightarrow 0) \propto n_s/m^*$ plotted against the planar Zn concentration in (Cu, Zn) substituted $YBa_2Cu_3O_{6.63}$ (123) and $La_{2-x}Sr_x(Cu, Zn)O_4$ with $x = 0.15$ and 0.20 [8]. The solid curve represents the variation expected for the 'Swiss cheese model' illustrated at the top, where superconductivity around each Zn is assumed to be destroyed in the area of $\pi\xi_{ab}^2$. (b) The gapped response (blue colour) versus normal state density of states (white colour) detected around one Zn impurity in (Cu, Zn) substituted Bi2212 by STM [9] (reproduced by permission of Nature Publishing Group http://www.nature.com). (c) The muon spin relaxation rate $\sigma(T \rightarrow 0) \propto n_s/m^*$ in Eu substituted $(La, Eu)_{1.85}Sr_{0.15}CuO_4$ plotted against the volume fraction V_{Cu} of Cu moments having static magnetic order [26]. The results demonstrate the trade-off between superconducting and magnetic volume fractions expected in the 'magnetic island formation' illustrated at the top. (d) The 'gap map' obtained by STM for moderately underdoped Bi2212 [10, 11]. The red–yellow regions represent the area where the sharp superconducting gap is observed, while the blue and black region has a response similar to those found in the 'pseudogap' region [68] or the non-superconducting, very underdoped region [69]. The characteristic length scale for this spontaneous formation of spatial heterogeneity is comparable to the coherence length ξ_{ab}.

Thus the nearly linear trend in figure 1 for all these systems represents a generic feature of the cuprate superfluid, which is impressively robust against the formation of spatial heterogeneity. This is a feature which we can expect for a superfluid of tightly bound bosons, as we shall see in the next section, but not for BCS systems where impurities can scatter an individual carrier before it experiences an attractive interaction with its pair in a retarded process.

5. Two-dimensional aspects

Let us now compare the cuprates with the superfluid transitions in thin films of ^{4}He and ^{4}He/^{3}He mixtures in regular and porous media. Figure 5(a) shows the temperature dependence

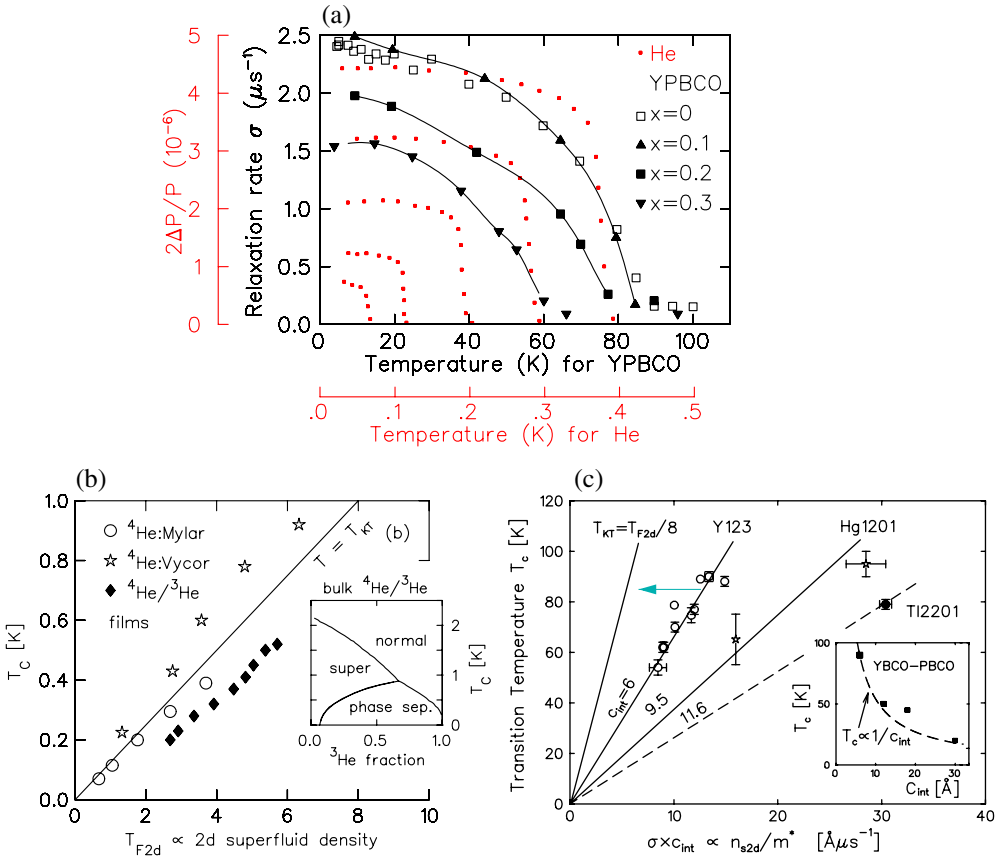

Figure 5. (a) Temperature dependences of the superfluid responses in a thin film of ^{4}He adsorbed on Mylar films (red points and axes) [51] compared with those in $(Y_{1-x}Pr_x)Ba_2Cu_3O_7$ (YPBCO) observed by means of μSR in unoriented [27] and oriented (multiplied by 1/1.4) [52] ceramic specimens. The solid curves are guides to the eye. (b) The superfluid transition temperature T_c versus the 2D superfluid density at $T \to 0$ for ^{4}He films on regular (Mylar) [51] and porous (Vycor) [54] media, and ^{4}He/^{3}He mixture films adsorbed on fine alumina powders [55] where the bulk phase separation in the inset is changed to microscopic heterogeneity via porous/powder media. The straight line represents values of the superfluid density jump expected at $T = T_c$ from the Kosterlitz–Thouless theory [46]. (c) T_c plotted against the 2D superfluid density $n_{s2D}/m^* \propto \sigma(T \to 0) \times c_{int}$ for various cuprate systems having different average interlayer spacings c_{int} [56]. The inset figure shows the T_c variation against c_{int} in MBE $YBa_2Cu_3O_7$ films where non-superconducting $PrBa_2Cu_3O_7$ was sandwiched with every unit cell along the c-axis direction [58]. The blue arrow illustrates the reduction of the superfluid density from the $T \to 0$ value towards the value expected at T_{KT}. The YBCO data in (a) show even further reduction from this 'T_{KT} jump' [57] value as T_c is approached.

of the superfluid density of a ^{4}He film on Mylar [51] and the relaxation rate $\sigma(T)$ in oriented optimally doped YBCO [52] (multiplied by a correction factor of 1/1.4) and (Y, Pr) substituted underdoped YBCO [27]. The superfluid density of ^{4}He film is almost independent of temperature until the KT transition suddenly drives the system into the normal state. In contrast, the superfluid density of YBCO shows a strong reduction with increasing T: the low-T variation was attributed to the excitation of nodal quasiparticles in the d-wave energy gap [53].

Figure 5(b) shows a plot of the superfluid transition temperature T_c versus the 2D superfluid density of ^{4}He films on regular (Mylar) [51] and porous (Vycor) [54] media and a ^{4}He/^{3}He mixture adsorbed on fine alumina powders [55]. The Mylar results represent the case with the smallest perturbation, comparable to that of the simple hole doped cuprates. The Vycor results are analogous to those for the Zn doped cuprates: normal regions are formed around the pore wall or around Zn impurities in order to help smooth the flow of the superfluid. The ^{4}He/^{3}He mixture corresponds to the overdoped cuprates, as discussed later. Despite the different degrees of perturbation, T_c precisely follows the linear relationship predicted by the Kosterlitz–Thouless theory [46]. The robustness against heterogeneity is common to the case of the cuprates in figure 1.

By multiplying the interlayer distance c_{int} by n_s/m^*, we can produce a corresponding plot for the cuprates with the horizontal axis representing the 2D area superfluid density n_{s2D}/m^*, as shown in figure 5(c) [56]. We find that:

(1) the systems with different c_{int} exhibit distinctly different slopes;
(2) the $T \to 0$ values of n_{s2D}/m^* are more than a factor of 2 larger than the 'KT jump' value $n_{s2D}/m^*(T = T_{KT})$ expected from the KT theory shown by the T_{KT} line [57]; and
(3) $T_c \propto 1/c_{int}$ from the early studies of YBCO/PrBCO sandwich layer systems [58].

These features indicate that the simplest version of the KT theory for two-dimensional systems is not adequate for accounting for the transition temperatures of cuprates. This point was missed in the argument of Emery and Kivelson [45].

For a non-interacting Bose gas with a parabolic energy dispersion, BE condensation does not occur in purely two-dimensional systems. However, one can expect condensation via inclusion of a small 3D coupling [47, 48] and/or dispersion with the power to k lower than 2 [59]. A small 3D coupling for a quasi-2D Bose gas would provide a logarithmic dependence of T_c on the coupling strength [47, 48], which decays exponentially with interlayer distance in the WKB approximation for the interlayer tunnelling. This would lead to the relation $T_c \propto n_{s2D}/m^* \times 1/c_{int} = n_s/m^*$ [56] which explains the trends in figures 1 and 5(c).

As illustrated in figure 5(c) with the blue arrow, the superfluid density of the cuprates is substantially reduced from the $T \to 0$ value before reaching the T_{KT} line, where the thermal creation of vortex/antivortex pairs could destroy the superconducting state if there is no interlayer coupling. For a substantial 3D coupling, the vortex pair creation is further suppressed, and $n_s/m^*(T)$ can be further reduced. Thus a key to understanding the correlations in figures 1 and 5(c) would be identifying the process which governs the thermal reduction of n_s/m^*.

6. Excitation: the magnetic resonance mode as a roton analogue

In bulk 3D superfluid ^{4}He, the transition temperature $T_c = 2.2$ K is determined by the phonon–roton dispersion relation shown in figure 6(a) [60]. The system loses superfluidity via this mechanism well below $T_{BE} = 3.2$ K. Although its energy $\hbar\omega_{rtn}$ corresponds to about $4k_BT_c$, the thermal excitation to the roton minimum has a large weight in the phase space thanks to a substantial momentum transfer of $\sim$2.0 Å^{-1}, and $\hbar\omega_{rtn}$ becomes a primary determining factor for T_c. This situation can be appreciated by looking at the linear relation between $\hbar\omega_{rtn}$ and T_c in bulk ^{4}He at different pressures [61], shown in figure 6(b), although only a small change is measurable.

It is then natural to search for a counterpart of the rotons in the cuprates. Here we propose the (π, π) $S = 1$ magnetic resonance mode, observed by means of neutrons, as excitations playing a role analogous to that of rotons. In figure 6(b), we plot T_c versus the energy of this mode $\hbar\omega_{res}$, determined by means of neutron scattering for various cuprate systems [15–18].

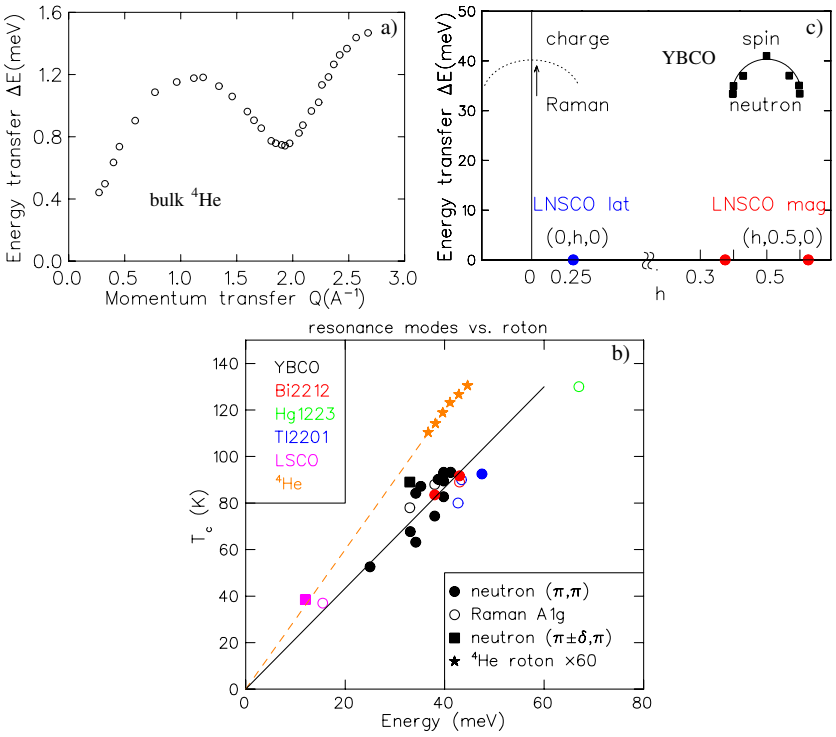

Figure 6. (a) The dispersion relation of phonon–roton excitations in superfluid ^{4}He observed by neutron scattering [60]. (b) A plot of T_c versus the energy of the roton minimum of bulk superfluid ^{4}He (values for both axes multiplied by a factor of 60) measured under applied pressures [61], compared with the relationship seen in HTSC systems for the energies of the neutron resonance mode at (π, π) [15–18] and the Raman $A1_g$ mode [19–22]. Also included are the neutron energy transfers at the $(\pi \pm \delta, \pi)$ point in YBCO [17] and LSCO [62]. (c) The dispersion relation around the (π, π) resonance mode observed in YBCO by means of neutrons [17] (closed circles), the location of the satellite Bragg peaks (red = magnetic; blue = lattice, estimated from the adjacent Brillouin zone) found in the static spin/charge stripe system $(La, Nd, Sr)_2CuO_4$ (LNSCO) [72], and the proposed charge branch of the hybrid spin/charge roton (dotted line), to which the Raman $A1_g$ response in (b) is ascribed.

We also include the peak energy $\hbar\omega_{A1g}$ of the $A1_g$ mode observed in Raman scattering [19–22], which closely follows the resonance mode energy. We see an impressive linear dependence of T_c on $\hbar\omega_{res}$ and $\hbar\omega_{A1g}$ for a wide variety of cuprates. The slopes of the linear relationships for cuprate resonances and He rotons are different by only 20% or so.

At a glance, we see that the magnetic resonance mode is quite different from rotons, since it does not create a liberated spin singlet charge pair or a charge density modulation, except through a mechanism which we will propose in the next section. However, the following argument may reveal further similarities between these excitations. The roton minimum represents a soft phonon mode, going towards solidification of He, which has not yet been achieved, at a momentum transfer close to that of the 'Bragg point of the solid He to be'. So, it can be viewed as an excitation mode directly related to the 'yet-to-be-stabilized ground state' competing with the superfluid ground state.

For underdoped cuprates, likely ground states competing against the superconducting state include the antiferromagnetic (AF) state and the stabilized incommensurate/stripe spin

state. Since the AF state develops around the momentum transfer (π, π), the $S = 1$ magnetic resonance mode can be viewed as an excitation related to this 'yet-to-be-achieved and competing ground state'. The stripe state develops around an incommensurate wavevector. Recently, the downward dispersion of the resonance mode towards this incommensurate wavevector was noticed in neutron studies [15, 62]. So, the incommensurate/stripe state could also be viewed as a competing ground state connected to the resonance mode. Indeed, in $La_2CuO_{4.11}$, the magnetic islands with stabilized incommensurate spin correlations coexist with surrounding superconducting and non-magnetic regions [25]. So, the superconducting and stripe states should have very close ground state energies and be competing with each other.

An important notion about rotons is that the excitation does not create the competing ground state itself, but populates 'excitations' associated with that competing state. The AF state or the incommensurate spin state is the spin singlet $S = 0$ state. So, the magnetic resonance mode represents the '$S = 1$ excited state' of the 'unachieved $S = 0$ AF state'. This is a way to understand the $S = 1$ excitation as an acceptable candidate roton analogue. 'Rotons as soft phonons' in ^{4}He are *excitations* associated with the unachieved solidified He lattice.

We also have to realize that the thermal excitations of the magnetic resonance mode could contribute towards reduction of the superfluid density n_s/m^*. This feature can be found in earlier 'spin exciton' theories of Norman and co-workers [63, 64] as well as the 'topological transition' theory of Onufrieva and Pfeuty [65]. Although the relationship to the superfluid density was not explicitly discussed in either theory, the resonance mode is described as a particle–hole excitation from the superconducting ground state. Thus the excitation of the resonance mode should reduce n_s/m^*. In other words, the superconducting ground state can be destroyed via excitations associated with the (yet-to-be-achieved) spin ordered state in the same way as those associated with charge ordered states. Now we can view the magnetic resonance mode in the cuprates as an excitation analogous to rotons in superfluid He as well as 'magneto-rotons' in fractional quantum Hall systems [66].

In the cuprates, the resonance mode energy is related to the 'distance from the competing ground state'. Thus $\hbar\omega_{res}$ increases with increasing doping as the system moves further away from the AF ordered state. It has been difficult to observe the resonance mode by means of neutron scattering in the La214 systems. However, if we adopt the Raman $A1_g$ results, T_c for the 214 system also follows a linear relation with the mode energy, as shown in figure 6(b). The resonance mode appears more clearly in the low-energy dispersion branch at the incommensurate position in LSCO [62]. In figure 5(b), we include the energy at $(\pi - \delta, \pi)$ for YBCO [17] and LSCO [62], which exhibits an even better agreement with the slope of the rotons.

In theoretical works on the resonance mode, we often find statements such as 'it is not known why the mode energy scales with T_c'. We claim here that T_c is determined by the mode energy via thermal excitations of the mode which reduce the superfluid density. The actual situation can, however, be somewhat more complicated since not only the resonance mode but also the 'continuum' excitations (or the $B1_g$ Raman modes) would contribute towards reduction of the superfluid density in the cuprates, and the energies of the resonance and continuum modes are very close to each other.

7. Reconciliation of Raman and neutron modes

Raman scattering usually probes spinless charge excitations at nearly zero net momentum transfer. How, then, can we explain the Raman $A1_g$ mode detection of the $S = 1$ magnetic resonance mode which involves spin flips and momentum transfer of (π, π)? This remains an open question. Possible but seemingly unlikely answers include a spin flip Raman mode

involving spin–orbit coupling, with detection of spin fluctuations near $k = 0$ within the 'shadow AF zone' dispersion corresponding to (π, π). A standard two-magnon Raman mode cannot explain the energy transfers of the Raman and neutron peaks being the same, since in that case the Raman $\hbar\omega_{A1g}$ should have been a factor of 2 larger than the neutron $\hbar\omega_{res}$. In superfluid ^{4}He, simultaneous creation of two rotons is known to give a strong Raman signal [67], ensuring momentum conservation with nearly opposite momentum transfers of the two rotons.

Recently, STM studies [11, 68, 69] found evidence for inelastic charge modulations spreading with the periodicity of four lattice constants, which could provide yet another relevant competing ground state. Lee and co-workers [70], and some other authors [71], proposed a picture involving a roton minimum for this charge density modulation. In general, any such charge or spin excitation relevant to competing ground states could play a role similar to the resonance mode as discussed here. However, we should note that the contribution of modes with small momentum transfers would provide a limited effect in the reduction of T_c due to its limited phase space factor. In this sense the (π, π) resonance mode is the most attractive candidate primary determining factor for T_c.

Struggling with the question of the almost identical energies of the $S = 1$ neutron resonance and presumably $S = 0$ Raman mode can give further insight into the roton-like mode in the cuprates. For $(La, Nd, Sr)_2CuO_4$, which shows stabilized stripe spin and charge modulations, neutron scattering [72] studies found magnetic incommensurate satellite Bragg peaks (red closed circle in figure 6(c)), separated from the AF zone centre (π, π) by a distance δ in momentum space due to spin modulation. Also observed simultaneously are the lattice deformation peaks at a distance 2δ from the lattice zone centre (blue closed circle in figure 6(c)), due to the charge modulation. Since the cuprate systems exhibit a preference for δ being $2\pi/8$, a spin/charge ordered stripe state with $\delta = 2\pi/8$ is a natural strong candidate 'competing ground state'. Having the periodicity $2\delta = 2\pi/4$, the charge modulation observed by STM could well be a manifestation of this stripe modulation or similar 2D incommensurate correlations in a dynamic response.

Suppose the superconducting ground state wins in the competition against this incommensurate state. This will lift the energies of both the magnetic and charge satellite Bragg peaks to finite energy transfers and create a magnetic resonance mode near the magnetic satellite as well as a charge modulation mode near the charge satellite. These spin and charge modes should coexist. The energy of these modes is determined by the energy difference between the superconducting state and the stripe state. Therefore, we would expect the *same energies* for the charge and spin modes, but these modes exist, of course, with different momentum transfers. This special situation creates a novel roton-like excitation in cuprates with double charge and spin minima, as illustrated in figure 6(c). We shall call this a 'hybrid spin/charge roton'.

This double-minima hybrid roton provides a natural resolution for the neutron versus Raman conflict. The $S = 1$ magnetic neutron mode is due to the spin branch while the Raman results can be understood as the manifestation of the charge/lattice branch, which would show up as the $S = 0$ response near the zone centre. It is then natural to find these modes with the same energy transfer, as is actually observed in experiments, as shown in figure 6(b).

Rotons are usually viewed as representing the density modulation in neutral superfluids and charge modulation in charged superconductors. The spin mode in cuprates, however, can exist only if the dynamic combined spin–charge modulation ensures that this mode is associated with the 'yet-to-be-achieved' static spin–charge modulated ground state. Therefore, the existence of the spin mode directly implies simultaneous dynamic charge modulation. This argument gives a basis for why the excitation of the magnetic resonance mode can contribute to the reduction of the superfluid density n_s/m^*, or in other words to the destruction of the superconducting order parameter, in the cuprates.

In charged superfluids and/or metals, the $k = 0$ response of the density fluctuations corresponds to plasmons, which usually exist at a rather high energy transfer. Then, one tends to presume a steep reduction of the charge roton branch towards the $2\delta = 2\pi/4$ minimum from the zone centre, instead of the rather modest energy reduction shown in figure 6(c). The in-plane plasma frequency ω_p at $k = 0$ for the optimally doped YBCO system, determined by means of optical conductivity [73], has an energy scale at least one order of magnitude higher than that of the 41 meV mode energy. This energy scale is also represented roughly by T_F obtained from the superfluid density, in figure 2, as the product of λ and ω_p is the light velocity. These energies represent 'real responses of the superconducting ground state'.

In the parent Mott insulator, all the charges are localized, and thus the plasma frequency is pushed down to zero, since the effective mass is infinitely large. Just as the magnetic mode energy represents the low-energy spin waves of the *yet-to-be-achieved Mott insulator AF state*, the charge branch in figure 6(c) should be considered for a *hypothetical situation* with a charge injected into a Mott insulator, somewhat comparable to the case of photoinduced conductivity experiments of a parent insulator system. Then, one might understand the very low energy scale, which could be related predominantly to nearly localized charges. There is another way to view the roton branches: suppose we temporarily create a small island region of the 'unachieved competing ground state', corresponding to a vacancy in the 'Swiss cheese', by supplying the finite energy transfer to the superconducting system, and study *excitations* within that island. Then we will find all the roton-like branches. This argument explains why the energy of the charge mode at the zone centre $k = 0$ can be identical to that of the magnetic mode at (π, π). More formally, this spin–charge coupling would provide terms analogous to the case of strong spin–orbit coupling, giving some qualification to the 'seemingly unlikely' argument of spin flip Raman scattering described at the beginning of this section. However, we will have to wait for further accumulation of experimental studies to clarify details of the 'charge branch' near the zone centre and its interplay with the lattice and spin degrees of freedom.

8. Phase separation in the overdoped region

In 1993, our group [24] and a European μSR team [30] independently found a very strange variation of n_s/m^* in overdoped Tl2201. As shown in figure 1, n_s/m^* decreases with increasing carrier doping, yet conductivity studies imply no anomaly in m^*. We presented a picture involving phase separation into superconducting and normal metal ground states [24, 7], while the authors of [30] interpreted this in terms of pair-breaking scattering. Coexistence of superconducting and normal charges at $T \to 0$ in Tl2201 also shows up in specific heat measurements by Loram *et al* [74], shown in figure 7(a). Upon overdoping from the highest-T_c sample in the nearly optimum region, the 'ungapped' response develops in the T-linear term $\gamma = C_{el}/T$ of the electronic specific heat C_{el}. As shown in figure 7(b), the 'gapped' fraction, presumably representing the volume fraction of the superconducting region, closely follows the variation of the superfluid response n_s/m^* obtained from the μSR [24].

Further evidence of coexisting gapped and ungapped ground states can be found in the height ΔC of the specific heat jump at T_c. For BCS superconductors, the height ΔC at T_c is proportional to T_c, as illustrated in figure 7(c). In the γ versus T plot, ideal BCS systems with different T_c values should exhibit the same jump height $\Delta C/T_c$, as illustrated in figure 7(d). Comparison of figures 7(a) and (d) reveals that the superconducting condensation in overdoped Tl2201 occurs only in a finite volume fraction. Thus the overdoped system is fundamentally different from standard BCS superconductors where all the normal state charge carriers participate in the superfluid n_s once the energy gap is developed around the entire

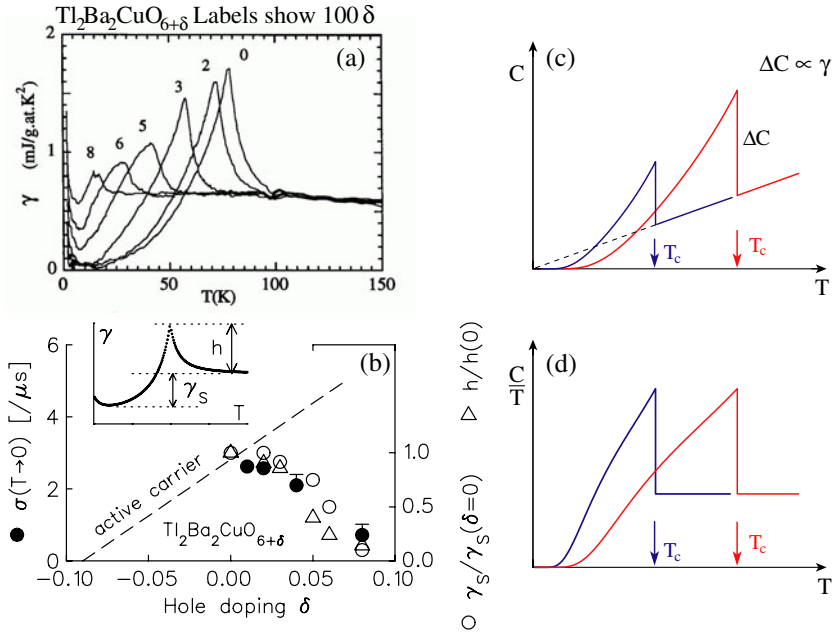

Figure 7. (a) The electronic specific heat observed by Loram *et al* [74] in the overdoped Tl2201 systems. (b) The variation of the μSR relaxation rate $\sigma(T \to 0)$ in Tl2201 [24] compared with the 'gapped' response γ_S (open circles) and the peak height h (open triangles) from the data in (a). (c) The specific heat jump in standard BCS superconductors with different T_c values. (d) As (c) but plotted as $\gamma = C/T$, to be compared to (a). Parts (a)–(d) together provide strong evidence for phase separation in the overdoped cuprates developing with increasing overdoping.

Fermi surface. The jump height $\Delta C/T_c$ follows the trend of n_s/m^* and the gapped volume fraction, as shown in figure 7(b), further reinforcing this argument.

Similar behaviours of the other overdoped cuprates have been found via subsequent μSR measurements on YBCO with (Y, Ca) substitution [75] and on CaLaBaCuO [31], and torque measurements on Hg1201 [76]. Other signatures of this anomaly include the ungapped response in the optical conductivity [77] in optimal to overdoped YBCO, and the recombination time of photoinduced antinodal quasiparticles which becomes independent of the laser excitation power in the overdoped region of Bi2212 [78]. All these results indicate that the overdoped cuprate systems have a substantial number of unpaired fermion carriers in the ground state. As condensed boson superfluids coexisting with fermionic carriers, the overdoped cuprates strongly resemble ^{4}He/^{3}He mixture films. Indeed the T_c versus n_s/m^* relationships in these two cases follow very similar behaviours, as shown in figures 1 and 5(b).

9. Phase diagrams and the Nernst effect

9.1. Phase diagrams

In recent years, we presented a generic phase diagram for the cuprates [79, 33], shown in figure 8(a), which is a hybrid of the BE–BCS conjecture and the phase separation picture in the overdoped region. We assume that the pairing energy, represented by T^*, vanishes *within* the superconducting dome at a critical concentration p_c in a modestly overdoped region. Tallon and Loram [80] obtained $p_c \sim 0.19$ holes per Cu for YBCO, Bi2212, and LSCO systems,

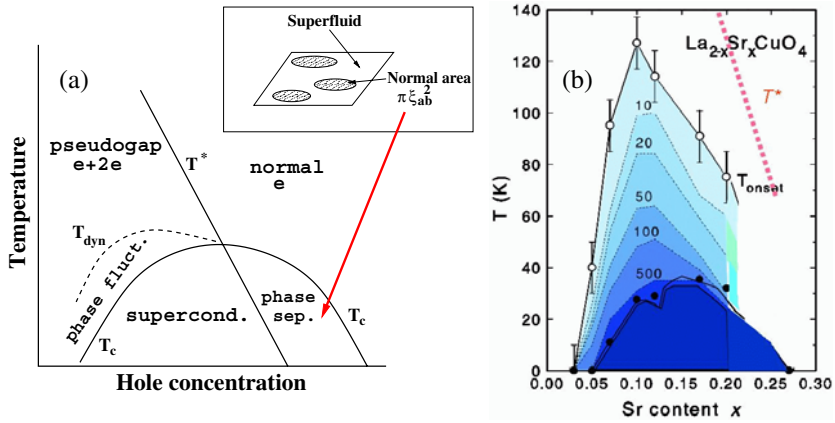

Figure 8. (a) A generic phase diagram proposed for cuprates by Uemura [33], including the distinction between the pair formation T^* and the onset temperature of dynamic superconductivity T_{dyn} which corresponds to T_{onset} for the Nernst effect. The inset illustrates the proposal of microscopic phase separation between superconducting and normal metal regions in the overdoped region [79]. (b) The region of the Nernst effect, shown in the T–x phase diagram for LSCO [83]. The result for T_{onset} for the $x = 0.10$ sample is plotted with the green star symbol in figure 2. The T^* values shown by the red dashed line are taken from [82].

while Hwang *et al* [81] obtained $p_c = 0.23$ for Bi2212, and another estimate [82] suggests that p_c could be even larger for LSCO, as illustrated in figure 8(b). These subtle differences may be partly due to the different definitions used for deriving T^* from results obtained by various experimental methods. It is also possible that p_c substantially varies from system to system.

In our view, the phase separation in the overdoped region occurs to save condensation and pairing energies at a cost of the (screened) Coulomb energy necessary for disproportionation of the charge density [79]. Without taking into account the possibility of phase separation, the authors of [80] and [81] argued that the existence of superconductivity at the hole concentration $x > p_c$ could rule out a positive role being played by the pseudogap state for superconductivity. Our phase separation picture, however, presents a counter-example and shows that the superconducting state can exist at $x > p_c$ with T^* representing the onset of an interaction *necessary* for superconductivity.

The reduction of T^* with increasing doping is well established from many experimental results. However, this is not a feature readily expected in a general argument on BE–BCS crossover. In fact, if the pair formation energy did not show a strong dependence on the doping, we could expect T_c to rise smoothly up to the T^* energy scale with increasing doping, after which the system slowly crosses over to a standard BCS behaviour with all the normal state carriers condensing in the superconducting state without spatial phase separation. T_c would still come down gradually in the high-density limit due to the effect of retardation. Compared to this 'standard BE–BCS crossover', the situation in the cuprates is different, because the 'origin of pairing interactions' seems to die away as the doping progresses.

9.2. The Nernst effect

The results on the high-frequency superconducting response [12] and the Nernst effect [13, 14] demonstrate the existence of vortex fluctuations (or 'superconducting phase fluctuations' or 'dynamic superconductivity') over a wide region of the normal state above T_c, as shown in figure 8(b) [83]. In thin films of ^{4}He, the corresponding region exists above the superfluid

temperature $T_c = T_{KT}$ up to the 'mean-field' superfluid energy scale whose upper limit can be given by the lambda transition temperature 2.2 K of bulk ^{4}He. This comparison leads us to realize that the 'Nernst region' could have been superconducting if the system was protected against various origins of destruction of the superconducting states, including low-dimensional aspects and excitation of roton-like modes, but all the other necessary characteristics for superconductivity were conserved. Then, the onset temperature T_{on} of the Nernst effect corresponds to T_c for such a 'hypothetical 3D and roton-less counterpart' of highly 2D cuprate systems.

In figure 2, we include a point (the green star) having T_F for $La_{1.9}Sr_{0.1}CuO_4$ on the horizontal axis and the Nernst onset T_{on} of the same system [13, 14] on the vertical axis. Interestingly, this point for 'hypothetical underdoped LSCO' lies very close to the T_{BE} line, similar to those of bulk ^{4}He and ultracold ^{40}K. This suggests that the effect of pair overlapping in the very underdoped region may be modest, and/or the coherence length could be comparable to the intercarrier distance. Indeed, the new estimate for ξ from the Nernst study [14] supports the latter picture.

For further doping, T_{on} is suppressed because T^* is reduced. It is important, however, to realize that the pair formation energy scale T^* and the onset of the dynamic superconductivity T_{on} represent two distinctly different energy scales on the BE side. Pair formation can occur at any high temperature if a strong attractive force is provided, while fluctuating superconductivity is possible only below T_{BE}. Observation of the Nernst effect above T_c does not distinguish between BE-type and BCS-type condensations, since a thin film of a typical BCS superconductor can also exhibit the Nernst effect above T_c. The more important feature for underdoped cuprates is the large region in the T–x phase diagram above T_{on} but below T^*, as shown in figures 8(a) and (b), where one would expect the emergence of normal but paired (2e) charge carriers coexisting with unpaired (e) carriers.

The observation of a Nernst effect above T_c does not necessarily imply KT-like phase fluctuations as the primary determining factor for T_c. In low-dimensional magnetic systems, we expect correlated spin fluctuations in a large temperature region above the 3D ordering temperature, for both cases—with or without a KT transition. Analogous to this, one can expect the Nernst effect for any superconducting system with strong anisotropy, where T_c is reduced from the 3D values but the transition temperature is still governed by the anisotropic coupling strength. Furthermore, excitations of roton-like modes would create liberated vortices and thus also contribute towards the Nernst signal.

9.3. The determining factor for T_c

In figure 1, the trajectory for the La214 systems exhibits 'early departure' from the straight line for YBCO and other cuprates. La214 systems have a particular closeness to competing magnetic ground states as demonstrated by the instability against spin/charge stripe formation near the 1/8 concentration. Thus, we can ascribe the reduced T_c (about a factor of 2 smaller than that for YBCO for a given n_s/m^*) to the reduced (and probably broadened) resonance mode energy.

For bulk superfluid ^{4}He, T_c is related to the particle density, the mass, and the roton energy. The roton energy provides a proper account for the reduction of T_c from T_{BE} due to the effects of finite boson size and interactions. In thin films of He, T_c is determined primarily by the particle density and mass via the KT transition, since the roton energy there would be much higher than T_{KT}. For underdoped cuprates, as we have seen, T_c seems to be related to the doped hole density and mass as well as to the resonance mode energy. The mode energy will become higher with hole doping as the system becomes distant from the AF state, while the increasing

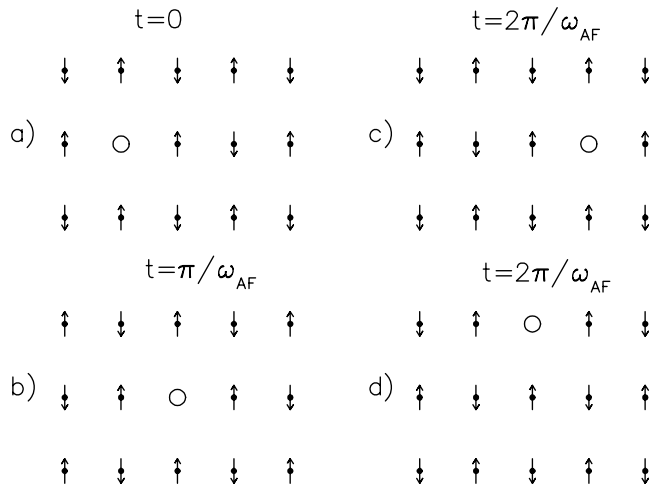

Figure 9. An illustration of a charge hopping motion in the cuprate resonant with the antiferromagnetic spin fluctuations with the frequency $\omega_{\rm AF}$. (a) is for the $t = 0$ configuration, (b) for $t = \pi/\omega_{\rm AF}$ after a half-period. (c) and (d) show the situation after the full period $t = 2\pi/\omega_{\rm AF}$ for the propagation towards the $(\pi, 0)$ direction and the (π, π) direction, respectively. The charge motion sequenced with AF spin fluctuations helps avoid extra frustration in the charge propagation process.

superfluid density would also help in lowering the energy of the superconducting state. Both of these factors would help in increasing $T_{\rm c}$ approximately linearly with the doping x.

However, the decrease of T^* with increasing x implies that the origin of superconducting pairing is destroyed gradually with increasing hole density x. In other words, the distance from the competing AF Mott insulator state helps increase the roton-like resonance energy while decreasing the coupling strength of superconducting pairs. This situation can be expected if the AF interaction provides the very origin of the pairing.

10. A microscopic model for pairing mediated by spin fluctuations

10.1. Motion of a charge resonating with AF spin fluctuations

Stimulated by this possibility, we now develop a microscopic model for a unique motion of a charge in nearly AF but actually metallic cuprate systems. Let us consider how a charge (hole) motion can avoid creating frustration in the region with short-range and dynamic AF correlations. We start with the situation for a single hole, illustrated in figure 9(a). The surrounding AF configuration is fluctuating with the frequency $\omega_{\rm AF}$, which implies that all the surrounding Cu spins change their directions within half a period $\pi/\omega_{\rm AF}$. If the charge hops to the adjacent site at this half-period, then there is no extra spin frustration in the surroundings; see figure 9(b). During the next half-period of spin fluctuations, the charge could hop further to the next adjacent site, as in figure 9(c). If the charge motion occurs this way, sequenced with the spin fluctuation, extra spin frustration can be avoided. Charge motion of any other (higher) frequency would lead to a mismatch with the spin lattice, and thus cost extra energy for creating frustrated magnetic bonds.

For a charge proceeding towards the Cu–O–Cu bond direction (i.e., the $(\pi, 0)$ direction in the reciprocal space), this implies that within the full period of spin fluctuations, the charge proceeds by two lattice constants. This charge motion has the wavevector $2\pi/2a$,

corresponding to that of the 'antinodal charge' at the $(\pi, 0)$ point of the Brillouin zone. So, the antinodal charge can proceed comfortably in the nearly AF environment, if its frequency (kinetic energy) 'resonates' with the frequency of the AF spin fluctuations. An especially strong spin–charge coupling can be expected for the case with $\hbar\omega_{\text{antinode}} = \hbar\omega_{\text{AF}}$.

This situation can be viewed as a charge motion creating the AF fluctuation with the frequency $\hbar\omega_{\text{AF}} = k_{\text{B}}T_{\text{F}}$, just as a motion of a charge in BCS superconductors creates a phonon. Analogous to BCS coupling mediated by a phonon, the creation of the AF fluctuating environment by the first charge motion in the cuprates can save the spin-frustration energy of the second charge upon its arrival. This would support coupled charges with a strong attractive interaction mediated by spin fluctuations.

In reciprocal space, this implies connecting the antinodal charges with AF fluctuation, as illustrated in figure 10(a). An initial charge at $(0, -\pi)$ creates a (π, π) AF fluctuation and ends up in a $(\pi, 0)$ charge in the final state. The same AF fluctuation can be absorbed by another charge having the initial state of $(0, \pi)$ which is scattered into $(-\pi, 0)$. The large energy gap in the antinodal positions, opening below T^*, would be a manifestation of the strong coupling of antinodal charges via this mechanism. In this case the spin fluctuations are analogous to phonons in BCS coupling, as a 'virtual' boson in the 'scattering' process. However, the direct coupling between the $(\pi, 0)$ and $(-\pi, 0)$ charges is not supported, since the AF (π, π) wavevector does not connect antinodal charges with opposite momentum directions.

10.2. Coupled nodal charges and the resonance mode as a pi-meson analogue

Let us now consider the motion of a single nodal charge at $(\pi/2, \pi/2)$ in the Brillouin zone. To achieve propagation along the nodal direction, this charge should hop, after the first hop in figure 9(b), towards the perpendicular direction from the first hop, leading to the state shown in figure 9(d) after one period of the AF spin fluctuation. In this case, the charge has moved a distance corresponding to the diagonal of the unit CuO_2 square lattice, with the corresponding wavevector (π, π) which is twice as large as that of the nodal carriers. Due to this complete mismatch, the single nodal carrier cannot benefit from the 'resonating motion'. However, the (π, π) AF fluctuation can connect two nodal charges, with opposite momentum directions, as shown in figure 10(b). This process provides a stable 'bound state' of two nodal charges, with the AF spin fluctuation playing the role of the Yukawa meson in the binding of hadrons in nuclei.

The energy of the AF fluctuation mediating this direct coupling is related to the size of the boson, similarly to the pion mass being related to the size of the deuteron nucleus, and also similarly to the energy gap being related to the coherence length in BCS superconductors. We note that the resonance mode energy of $\sim$41 meV is entirely appropriate for creating a boson having the size of the coherence length $\sim$10–20 Å in the cuprates. Thus we suggest the possibility that the magnetic resonance mode could be the pair mediating boson for nodal charges.

10.3. Nodal versus antinodal carriers and the ARPES coherence peak

As discussed in earlier sections, we also expect the existence of 'a charge branch' of the hybrid spin/charge roton, and/or higher-energy charge fluctuations, which could cause scattering of nodal charges with a rather small momentum change within the 'nodal hole pocket', as shown in figure 10(d), to contribute to an additional scattering process for an attractive interaction. Nearly AF spin fluctuations can also contribute to this type of scattering process between the two different nodal hole pockets across the zone centre, in addition to the direct binding.

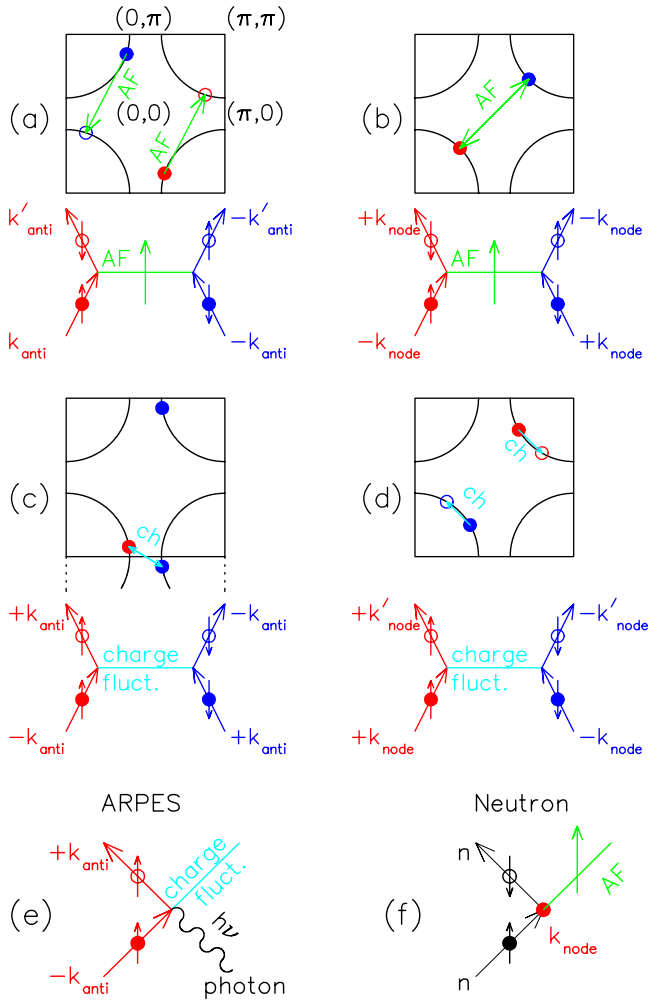

Figure 10. An illustration of the attractive interaction obtained in the scattering processes (a) and (d), and in the binding processes (b) and (c), involving the exchange of AF spin fluctuations and charge fluctuations in the cuprates. (e) and (f) show the diagrams for the ARPES coherence peak [23] for antinodal charges (e), and the neutron resonance peak for nodal charges (f), which can be viewed as processes liberating Yukawa-type bonding bosons. These liberation processes occur at a cost of condensation energy, corresponding to the hybrid spin/charge roton energy, with the intensities proportional to the superfluid density n_s/m^*. (a), (c) and (e) show processes for the antinodal charges, while (b), (d) and (f) show those for nodal charges.

When the charge branch excitation couples two antinodal particles near the $(0, -\pi)$ points, one of them can be viewed as a $(0, +\pi)$ particle in an Umklapp process, as illustrated in figure 10(c). Then the charge branch roton can be the direct 'binding boson' of antinodal charges, similarly to the spin branch case for nodal charges. Since the ARPES measurements probe $S = 0$ charge processes with no spin flip, and since the coherence peak selectively appears in antinodal responses, the ARPES coherence peak can be viewed as reflecting the process of detecting/liberating the charge branch roton via energy supplied by a photon, analogous to the Raman $A1_g$ mode. Figures 10(e) and (f) compare this process with neutrons creating

the magnetic resonance mode for nodal particles. In these 'liberation processes' for binding bosons, we expect the intensity to be proportional to the number of condensed bosons. This is similar to pion creation with accelerated particle beams, in which the intensity is proportional to the number of nucleons existing in the production target. This argument explains why the ARPES coherence peak and neutron resonance peak both appear with intensities proportional to the superfluid density n_s/m^*.

The interplay between the 'scattering' process (figures 10(a) and (d)) and the 'binding' process (figures 10(b) and (c)) is reminiscent of the Feshbach resonance [40, 84] appearing in the BE–BCS crossover of ultracold atoms. Note that some of these processes in figure 10, such as the binding ones in (b) and (c), may take place simultaneously/cooperatively as combined spin/charge fluctuations, as discussed earlier. In the Hamiltonian of such coupled processes, the spin fluctuation operator (the green line in figure 10) and the charge fluctuation operator (the light blue line) might appear together, operating simultaneously on the wavefunction composed of a combination of the nodal and antinodal wavefunctions. This strong spin–charge coupling may not be confined to the case of the low-energy hybrid roton in (b) and (c), but could also exist in scattering processes with higher-energy fluctuations shown in (a) and (d). Then we expect high-energy charge fluctuations to appear with the same energy transfers as the high-energy AF spin fluctuations spreading over the energy region up to about 100–200 meV or so. The inelastic charge modulation recently observed by STM appears exactly in this energy region with the momentum transfer close to that of the charge branch of the hybrid roton. Thus, this STM signature can be viewed as a manifestation of the counterpart of the AF spin fluctuations. Other possible signatures of the corresponding dynamic charge modulations include the line profile of ARPES antinodal intensities near 100–150 meV, and the 'mid-infrared reflection' observed in optical conductivity measurements in this energy region.

Being originally antiferromagnetic localized spins, the antinodal carriers may have a rather high effective mass, and thus may make a limited contribution to the superfluid spectral weight n_s/m^*. Nodal charges are directly originating from doped holes, and known to support a rather high normal state conductivity, suggestive of a light mass. It looks as if the antinodal charges are helping with the propagation of nodal pairs by creating large energy gaps, while the main superfluid spectral weight comes from the nodal pairs. This picture gives a natural explanation for n_s/m^* being nearly proportional to the doped (mobile) carrier concentration. Our model of coupled spin/charge operators suggests that the nodal and antinodal responses are strongly coupled, and cannot exist separately. The detailed roles and interplay of these two different regions of the Fermi surface are, however, yet to be clarified and will require future research.

10.4. Retardation and the phase diagram

In figure 3(b), we proposed the BE–BCS crossover region to have $k_B T_F$ comparable to the energy of the pair mediating boson $\hbar\omega_B$ in a rather arbitrary discussion based on the 'retardation' concept. If we assume that the 'optimal doping' region of the cuprates represents the crossover region, this argument suggests that $k_B T_F \sim 2000$ K for the optimally doped YBCO could represent the energy scale of the pair mediating bosons. This crude estimate is consistent with spin fluctuations as a pair mediator [56], since $\hbar\omega_{AF}$ develops over the energy region up to the AF exchange interaction $J \sim 1200$–1500 K.

Furthermore, our argument of 'resonant charge motion' can work only when the charge energy scale does not exceed the spin fluctuation energy scale. Doping further carriers into the overdoped region would increase the energy scale of doped normal holes exceeding the spin fluctuation energy scales. Then we cannot expect any more 'resonant charge motion' or 'pairing mediated by spin fluctuations'. This provides reasoning from the microscopic model

for why the crossover region appears at $k_B T_F \sim \hbar\omega_{AF}$, and why superconductivity in the overdoped region becomes progressively weaker with anomalous coexistence of paired and unpaired charges.

11. Discussion and conclusions

In our model, the closeness to the competing ground state can be a factor reducing T_c (by reducing the resonance roton minimum energy) and thus destructive to superconductivity, as well as a factor necessary for superconductivity in supplying mediating bosons in scattering and binding processes. This dual role of the competing ground state provides the very origin of the 'dome-like phase diagram', and also determines the distance of the maximum T_c from the T_{BE} line in figure 2. Although various different non-cuprate superconductors in figure 2 could have different 'competing ground states', a similar situation might exist in most of the systems originating from Mott insulators, which could in the future provide some account of why their T_c is limited to an apparently universal maximum value of $T_c/T_F \sim 0.05$; see figure 2.

There have been two different schools of thought as regards explaining the superconductivity of cuprates. One assumes the condensation of pre-formed pairs in the underdoped region, which is somehow perturbed in the overdoped region. The other starts from 'strong' superconductivity in the overdoped region and views it as being gradually destroyed with decreasing carrier density in the competition against other (presumably more magnetic) ground states in the underdoping region. Although still based on the former viewpoint, the present picture qualitatively describes how to account for the effect of 'competing ground states', and reconciles some conflict between these two views.

In theoretical discussions of HTSC or one-dimensional systems, 'spin–charge separation' is often the key underlying concept. Our model of charge propagation, resonant with spin fluctuations, provides a new way out of the spin–charge separation problem and out of associated spin frustration. We pointed out several observations as evidence for extremely strong spin–charge coupling, which leads to superconductivity of the cuprates. The strong involvement of the charge degrees of freedom in pairing could help in interpretation of the isotope effect [85] and other signatures of lattice involvements, such as the 'kink' in the electronic dispersion found in ARPES studies [86].

In summary, we have elucidated the role of superfluid density via accumulated μSR results and proposed the roton-like resonance mode as a primary determining factor of T_c. On the underdoped side, these two parameters, n_s/m^* and $\hbar\omega_{res}$, combine to determine T_c in a way very similar to that in superfluid bulk ^{4}He. In the 214 system, close to competing ground states, the strong effect of reduced $\hbar\omega_{res}$ causes the early departure of the points in figure 1 from the nearly linear trend of other systems. We proposed a few new pictures including:

(1) 'hybrid spin–charge roton', to reconcile selection rules of neutron and Raman modes;
(2) a microscopic model which explains how the charge motion and AF spin fluctuations can be coupled, in a sequential resonating way, to create an attractive interaction among antinodal and nodal charges;
(3) the possibility that the magnetic resonance mode plays a role of bonding bosons, analogous to pi-mesons, which bind two nodal charges; and
(4) the ARPES coherence peak and Raman $A1_g$ mode can be viewed as manifestations of the charge branch of the hybrid spin/charge roton.

We also demonstrated the robustness of the superconductivity in the cuprates against spatial heterogeneity, analogous to the superfluid He film case, as an essential feature which cannot be expected in BCS superconductors. We hope that these pictures elucidate the fundamental

importance of the BE condensation concept for the cuprates and provide useful conceptual frameworks for understanding their unique condensation and pairing aspects.

Acknowledgments

The work at Columbia was supported by the NSF DMR-0102752 INT-0314058 and CHE-0111752 (Nanoscale Science and Engineering Initiative). Some of the ideas in this paper were developed during the author's stay in IMR, Tohoku University, Japan, as a Visiting Professor, during January–March, 2003. The author wishes to thank Bob Laughlin and Naoto Nagaosa for useful discussions. The author has had an intuitive view of interpreting the magnetic resonance mode as a 'roton-like' excitation for the past three years or so, based on the energy analogy shown in figure 6(b). When he confessed this idea as a wild speculation to these two scientists in the spring of 2003, they kindly pointed out several difficulties with this speculation. Struggles to resolve some of them led the author to develop the picture detailed in this paper. The author would also like to thank Oleg Tchernyshyov for very illuminating discussions, J C Seamus Davis for sending the STM results on the charge modulation [11], and Graeme Luke and many other scientists for their collaborations in our 17 years of μSR studies on high-T_c superconductivity.

References

[1] 1979 *Hyperfine Interact.* **6**
1981 *Hyperfine Interact.* **8**
1984 *Hyperfine Interact.* **17–19**
1986 *Hyperfine Interact.* **31**
1990 *Hyperfine Interact.* **63–65**
1994 *Hyperfine Interact.* **85–87**
1997 *Hyperfine Interact.* **104–106**
2000 *Physica* B **289/290**
2002 *Physica* B **326**

[2] For a general review of μSR, see, for example, Schenck A 1985 *Muon Spin Rotation Spectroscopy* (Bristol: Hilger)

[3] For a recent reviews of μSR studies in topical subjects, see Lee S L, Kilcoyne S H and Cywinski R (ed) 1999 *Muon Science: Muons in Physics, Chemistry and Materials. Proc. 51st Scottish Universities Summer School in Physics (St Andrews, Aug. 1988)* (Bristol: Institute of Physics Publishing)

[4] Uemura Y J *et al* 1989 Universal correlations between T_c and n_s/m^* (carrier density over effective mass) in high-T_c cuprate superconductors *Phys. Rev. Lett.* **62** 2317

[5] Uemura Y J *et al* 1991 Basic similarities among cuprate, bismuthate, organic, chevrel-phase and heavy-fermion superconductors shown by penetration-depth measurements *Phys. Rev. Lett.* **66** 2665

[6] Uemura Y J 1995 Energy scales of exotic superconductors *Polarons and Bipolarons in High-T_c Superconductors and Related Materials. Proc. Int. Workshop on Polarons and Bipolarons in High-T_c Superconductors and Related Materials (Cambridge, UK, April 1994)* ed E Salje, A S Alexandrov and Y Liang (Cambridge: Cambridge University Press) pp 453–60

[7] Uemura Y J 1995 Energy scales of high-T_c cuprates, doped fullerenes, and other exotic superconductors *Proc. Int. Symp./Workshop on High-T_c Superconductivity and the C_{60} Family (Beijing, May 1994)* ed H C Ren (New York: Gordon and Breach) pp 113–42

[8] Nachumi B *et al* 1996 Muon spin relaxation studies of Zn-substitution effects in high-T_c cuprate superconductors *Phys. Rev. Lett.* **77** 5421

[9] Pan S H, Hudson E W, Lang K M, Eisaki H, Uchida S and Davis J C 2000 Imaging the effects of individual zinc impurity atoms on superconductivity in $Bi_2Sr_2CaCu_2O_{8+\delta}$ *Nature* **403** 746

[10] Lang K M, Madhavan V, Hoffman J E, Hudson E W, Eisaki H, Uchida S and Davis J C 2002 Imaging the granular structure of high-Tc superconductivity in underdoped $Bi_2Sr_2CaCu_2O_{8+\delta}$ *Nature* **415** 412

[11] McElroy K, Lee D-H, Hoffman J E, Lang K M, Lee J, Hudson E W, Eisaki H, Uchida S and Davis J C 2004 Detection of heterogeneous charge order coexisting with homogeneous nodal superconductivity in strongly underdoped $Bi_2Sr_2CaCu_2O_{8+\delta}$ *Preprint* cond-mat/0404005
[12] Corson J, Mallozzi R, Orenstein J, Eckstein J N and Bozovic I 1999 Vanishing of phase coherence in underdoped $Bi_2Sr_2CaCu_2O_{8+\delta}$ *Nature* **398** 221
[13] Xu Z A, Ong N P, Wang Y, Kakeshita T and Uchida S 2000 Vortex-like excitations and the onset of superconducting phase fluctuation in underdoped $La_{2-x}Sr_xCuO_4$ *Nature* **406** 486
[14] Wang Y, Ono S, Onose Y, Gu G, Ando Y, Tokura Y, Uchida S and Ong N P 2003 Dependence of upper critical field and pairing strength on doping in cuprates *Science* **299** 86
[15] Rossat-Mignod J, Regnault L P, Vettier C, Bourges P, Burlet P, Bossy J, Henry J Y and Lapertot G 1991 Neutron scattering study of the $YBa_2Cu_3O_{6+x}$ system *Physica* C **185–189** 86
[16] Fong H F, Keimer B, Reznik D, Milius D L and Aksay I A 1996 Polarized and unpolarized neutron-scattering study of the dynamic spin susceptibility of $YBa_2Cu_3O_7$ *Phys. Rev.* B **54** 6708
[17] Bourges P, Sidis Y, Fong H F, Regnault L P, Bossy J, Ivanov A and Keimer B 2000 The spin excitation spectrum in superconducting $YBa_2Cu_3O_{6.85}$ *Science* **288** 1234
[18] Sidis Y, Pailhés S, Keimer B, Bourges P, Ulrich C and Regnault L P 2004 Magnetic resonant excitation in high-T_c superconductors *Preprint* cond-mat/0401328
[19] Gallais Y, Sacuto A, Bourges P, Sidis Y, Forget A and Colson D 2002 Evidence for two distinct energy scales in the Raman spectra of $YBa_2(Cu_{1-x}Ni_x)_3O_{6.95}$ *Phys. Rev. Lett.* **88** 177401 and references therein
[20] Misochko O V and Gu G 1999 Electronic Raman scattering in disordered $Bi_2Sr_2Ca(Cu_{1-y}Fe_y)_2O_\delta$: impurity scattering effects *Phys. Rev.* B **59** 11183
[21] Gasparov L V, Lemmens P, Brinkmann M, Kolesnikov N N and Günterodt G 1997 Electronic Raman scattering in the single CuO_2 layered superconductor $Ta_2Ba_2CuO_{6+\delta}$ *Phys. Rev.* B **55** 1223
[22] Chen X K, Irwin J C, Trodahl H J, Kimura T and Kishio K 1994 Investigation of the superconducting gap in $La_{2-x}Sr_xCuO_4$ by Raman spectroscopy *Phys. Rev. Lett.* **73** 3290
[23] Feng D L *et al* 2000 Signature of superfluid density in the single-particle excitation spectrum of $Bi_2Sr_2CaCu_2O_{8+\delta}$ *Science* **289** 277
[24] Uemura Y J *et al* 1993 Magnetic field penetration depth in $Tl_2Ba_2CuO_{6+\delta}$ in the overdoped regime *Nature* **364** 605
[25] Savici A T *et al* 2002 Muon spin relaxation studies of incommensurate magnetism and superconductivity in stage-4 $La_2CuO_{4.11}$ and $La_{1.88}Sr_{0.12}CuO_4$ *Phys. Rev.* B **66** 014524
[26] Kojima K M, Uchida S, Fudamoto Y, Gat I M, Larkin M I, Uemura Y J and Luke G M 2003 Superfluid density and volume fraction of static magnetism in stripe-stabilized $La_{1.85-y}Eu_ySr_{0.15}CuO_4$ *Physica* B **36** 316–20
[27] Seaman C L *et al* 1990 Magnetic penetration depth of $Y_{1-x}Pr_xBa_2Cu_3O_{6.97}$ measured by muon-spin relaxation *Phys. Rev.* B **42** 6801
[28] Pümpin B, Keller H, Kündig W, Savić I M, Schneider J W, Simmer H, Zimmermann P, Kaldis E, Rusiecki S and Rossel C 1990 μSR in oxygen deficient $YBa_2Cu_3O_x$ ($6.5 \leqslant x \leqslant 7.0$) *Hyperfine Interact.* **63** 25
[29] Tallon J L, Bernhard C, Binninger U, Hofer A, Williams G V M, Ansaldo E J, Budnick J I and Niedermayer Ch 1995 In-plane anisotropy of the penetration depth due to superconductivity on the Cu–O chains in $YBa_2Cu_3O_{7-\delta}$, $Y_2Ba_4Cu_7O_{15-\delta}$, and $YBa_2Cu_4O_8$ *Phys. Rev. Lett.* **74** 1008
[30] Niedermayer Ch, Bernhard C, Binninger U, Glückler H, Tallon J L, Ansaldo E J and Budnick J I 1993 Muon spin rotation study of the correlation between T_c and n_s/m^* in overdoped $Tl_2Ba_2CuO_{6+\delta}$ *Phys. Rev. Lett.* **71** 1764
[31] Keren A, Kanigel A, Lord J S and Amato A 2003 Superconductivity and magnetism in $(Ca_xLa_{1-x})(Ba_{1.75-x}La_{0.25+x})Cu_3O_y$: a μSR investigation *Solid State Commun.* **126** 39
[32] Bardeen J, Cooper L N and Schrieffer J R 1957 Theory of superconductivity *Phys. Rev.* **108** 1175
[33] Uemura Y J 2003 Superfluid density of high-T_c cuprate systems: implication on condensation mechanisms, heterogeneity and phase diagrams *Solid State Commun.* **126** 23
Uemura Y J 2003 *Solid State Commun.* **126** 425 (erratum)
[34] Barford W and Gunn J M F 1988 The theory of the measurements of the London penetration depth in uniaxial type-II superconductors by muon spin rotation *Physica* C **156** 515
[35] Uemura Y J *et al* 1991 Magnetic field Penetration depth in K_3C_{60} measured by muon spin relaxation *Nature* **352** 605
[36] Uemura Y J, Keren A, Le L P, Luke G M, Wu W D, Tsai J S, Tanigaki K, Holczer K, Donovan S and Whetten R L 1994 System dependence of the magnetic-field penetration depth in C_{60} superconductors *Physica* C **235–240** 2501
[37] Le L P *et al* 1992 Muon-spin-relaxation measurements of magnetic penetration depth in organic superconductors (BEDT-TTF)$_2-$X: X = Cu(NCS)$_2$ and Cu[N(CN)$_2$]Br *Phys. Rev. Lett.* **68** 1923

[38] Uemura Y J *et al* 2000 μSR studies of intercalated HfNCl superconductors *Physica* B **289** 389
[39] Uemura Y J *et al* 2004 Unconventional superconductivity in $Na_{0.35}CoO_2 \cdot 1.3D_2O$ and proximity to a magnetically ordered phase *Preprint* cond-mat/0403031
[40] Regal C A, Greiner M and Jin D S 2004 Observation of resonance condensation of fermionic atom pairs *Phys. Rev. Lett.* **92** 040403
[41] Nozières P and Schmitt-Rink S 1985 Bose condensation in an attractive fermion gas—from weak to strong coupling superconductivity *J. Low Temp. Phys.* **59** 195
[42] Alloul H, Ohno T and Mendels P 1989 ^{89}Y NMR evidence for a Fermi-liquid behavior in $YBa_2Cu_3O_{6+x}$ *Phys. Rev. Lett.* **63** 1700
[43] Takigawa M, Reyes A P, Hammel P C, Thompson J D, Heffner R H, Fisk Z and Ott K C 1991 Cu and O NMR studies of the magnetic properties of $YBa_2Cu_3O_{6.63}$ ($T_c = 62$ K) *Phys. Rev.* B **43** 247
[44] Ito T, Takagi H, Ido T, Ishibashi S and Uchida S 1991 Normal state conductivity between CuO_2 planes in copper-oxide superconductors *Nature* **350** 596
[45] Emery V and Kivelson S 1995 Importance of phase fluctuations in superconductors with small superfluid density *Nature* **374** 434
[46] Kosterlitz J M and Thouless D J 1973 Ordering, metastability and phase-transitions in 2-dimensional systems *J. Phys. C: Solid State Phys.* **6** 1181
[47] Friedberg R and Lee T D 1989 Gap energy and long-range order in the boson–fermion model of superconductivity *Phys. Rev.* B **40** 6745
[48] Friedberg R, Lee T D and Ren H C 1991 Application of the s-channel theory to the μSR and Hall number experiments on high-T_c superconductors *Phys. Lett.* A **152** 423
[49] Randeria M 1995 Crossover from BCS theory to Bose–Einstein condensation *Bose–Einstein Condensation* ed A Griffin, D W Snoke and S Stringari (Cambridge: Cambridge University Press) pp 355–91 and references therein
[50] Uchida S 2003 Critical points in the cuprate phase diagram *Solid State Commun.* **126** 57
[51] Agnolet G, McQueeney D F and Reppy J D 1989 Kosterlitz–Thouless transition in helium films *Phys. Rev.* B **39** 8934
[52] Uemura Y J *et al* 1988 μSR studies on high-T_c superconductivity *J. Physique Coll.* **49** C8 2087
[53] Sonier J E, Brewer J H and Kiefl R F 2002 μSR studies of the vortex state in type-II superconductors *Rev. Mod. Phys.* **72** 769
[54] Bishop D J, Berthold J E, Parpia J M and Reppy J D 1981 Superfluid density of thin ^{4}He films adsorbed in porous Vicor glass *Phys. Rev.* B **24** 5047
[55] Chyo H and Williams G A 1998 Superfluid phase transition of ^{3}He–^{4}He mixture films adsorbed on alumina powder *J. Low Temp. Phys.* **110** 533
[56] Uemura Y J 1997 Bose–Einstein to BCS crossover picture for high-T_c cuprates *Physica* C **282–287** 194
[57] Bishop D J and Reppy J D 1978 Study of superfluid transition in 2-dimensional He-4 films *Phys. Rev. Lett.* **40** 1727
[58] Fisher Ø, Triscone J M, Brunner O, Antognazza L, Affronte M, Eibt O, Miéville L, Boichat T and Karkut M G 1991 Superconductivity in artificially grown copper-oxide superlattices *Physica* B **169** 116
[59] Aguilera-Navarro V C, de Llano M and Solis M A 1999 Bose–Einstein condensation for general dispersion relations *Eur. J. Phys.* **20** 177
[60] Henshaw D G and Woods A D B 1961 Modes of atomic motions in liquid helium by inelastic scattering of neutrons *Phys. Rev.* **121** 1266
[61] Dietrich O W, Graf E H, Huang C H and Passell L 1972 Neutron scattering by rotons in liquid helium *Phys. Rev.* A **5** 1377
[62] Christensen N B, McMorrow D F, Rønnow H M, Lake B, Hayden S, Aeppli G, Perring T G, Mangkorntong M, Nohara M and Takagi H 2004 Universal dispersive excitations in the high-temperature superconductors *Preprint* cond-mat/0403439
[63] Norman M R and Pepin C 2003 The electronic nature of high temperature cuprate superconductors *Preprint* cond-mat/0302347
[64] Eschrig M and Norman M R 2003 Effect of the magnetic resonance on the electronic spectra of high-T_c superconductors *Phys. Rev.* B **67** 144503
[65] Onufrieva F and Pfeuty P 2002 Spin dynamics of a two dimensional metal in a superconducting state: application to the high-T_c cuprates *Phys. Rev.* B **65** 054515 and references therein
[66] Girvin S M, MacDonald A H and Platzman P M 1986 Magneto-roton theory of collective excitations in the fractional quantum Hall effect *Phys. Rev.* B **33** 2481
[67] Greytak T J, Woerner R, Yan J and Benjamin R 1970 Experimental evidence for a two-roton bound state in superfluid helium *Phys. Rev. Lett.* **25** 1547

[68] Vershinin M, Misra S, Ono S, Abe Y, Ando Y and Yazdani A 2004 Local ordering in the pseudogap state of the high-T_c superconductor $Bi_2Sr_2CaCu_2O_{8+\delta}$ *Science* **303** 1995–8
[69] Hanaguri T, Lupien C, Kohsaka Y, Lee D-H, Azuma M, Takano M, Takagi H and Davis J C 2004 Discovery of a 'checkerboard' electronic crystal phase in the lightly doped Mott insulator $Ca_{2-x}Na_xCuO_2Cl_2$ *Preprint*
[70] Fu H C, Davis J C and Lee D H 2004 On the charge ordering observed by recent STM experiments *Preprint* cond-mat/0403001
[71] Nazario Z and Santiago D I 2004 Roton induced modulations in underdoped cuprates as a signature of incipient electronic order *Preprint* cond-mat/0403374
[72] Tranquada J M, Sternlieb B J, Axe J D, Nakamura Y and Uchida S 1995 Evidence for stripe correlations of spins and holes in copper-oxide superconductors *Nature* **375** 561
[73] Homes C C, Bonn D A, Liang R, Hardy W N, Basov D N, Timusk T and Clayman B P 1999 Effect of Ni impurities on the optical properties of $YBa_2Cu_3O_{6+y}$ *Phys. Rev.* B **60** 9782
[74] Loram J W, Mirza K A, Wada J M, Cooper J R and Liang W Y 1994 The electronic specific heat of cuprate superconductors *Physica* C **235–240** 134
[75] Bernhard C, Tallon J L, Blasius Th, Golnik A and Niedermayer Ch 2001 Anomalous peak in the superconducting condensate density of cuprate high-T_c superconductors at a unique doping state *Phys. Rev. Lett.* **86** 1614
[76] Hofer J, Karpinski J, Willemin M, Meijer G I, Kopnin E M, Molinski R, Schwer H, Rossel C and Keller H 1998 Doping dependence of superconducting parameters in $HgBa_2CuO_{4+d}$ single crystals *Physica* C **297** 103
[77] Schützmann J, Tajima S, Miyamoto S and Tanaka S 1994 *c*-axis optical response of fully oxygenated $YBa_2Cu_3O_{7-\delta}$: observation of dirty-limit-like superconductivity and residual unpaired carriers *Phys. Rev. Lett.* **73** 174
[78] Gedik N and Orenstein J 2004 private communication
[79] Uemura Y J 2001 Microscopic phase separation in the overdoped region of high-T_c cuprate superconductors *Solid State Commun.* **120** 347
[80] Tallon J L and Loram J W 2001 The doping dependence of T^*—what is the real high-T_c phase diagram? *Physica* C **349** 53
[81] Hwang J, Timusk T and Gu G D 2004 High-transition-temperature superconductivity in the absence of the magnetic resonance mode *Nature* **427** 715
[82] Timusk T and Statt B 1999 The pseudogap in high temperature superconductors: an experimental survey *Rep. Prog. Phys.* **62** 61
[83] Wang Y, Xu Z A, Kakeshita T, Uchida S, Ono S, Ando Y and Ong N P 2001 Onset of the vertexlike Nernst signal above T_c in $La_{2-x}Sr_xCuO_4$ and $Bi_2Sr_{2-y}La_yCuO_6$ *Phys. Rev.* B **64** 224519
[84] Inouye S, Andrews M R, Stenger J, Miesner H J, Stamper-Kurn D M and Ketterle W 1998 Observation of Feshbach resonances in a Bose–Einstein condensate *Nature* **392** 151
[85] Khasanov R, Shengelaya A, Morenzoni E, Conder K, Savić I M and Keller H 2004 Oxygen-isotope effect on the in-plane penetration depth in cuprate superconductors *Preprint* cond-mat/0404428
[86] Damascelli A, Hussain Z and Shen Z X 2003 Angle-resolved photoemission studies of the cuprate superconductors *Rev. Mod. Phys.* **75** 473